

Low-temperature sequential pulsed chemical vapor deposition of ternary $B_xGa_{1-x}N$ and $B_xIn_{1-x}N$ thin film alloys

Ali Haider, Seda Kizir, Cagla Ozgit-Akgun, Ali Kemal Okyay, and Necmi Biyikli

Citation: *Journal of Vacuum Science & Technology A* **34**, 01A123 (2016); doi: 10.1116/1.4936072

View online: <http://dx.doi.org/10.1116/1.4936072>

View Table of Contents: <http://scitation.aip.org/content/avs/journal/jvsta/34/1?ver=pdfcov>

Published by the AVS: Science & Technology of Materials, Interfaces, and Processing

Articles you may be interested in

Effects of growth temperature on the properties of InGaN channel heterostructures grown by pulsed metal organic chemical vapor deposition

AIP Advances **5**, 127102 (2015); 10.1063/1.4937127

Optical characteristics of nanocrystalline $Al_xGa_{1-x}N$ thin films deposited by hollow cathode plasma-assisted atomic layer deposition

J. Vac. Sci. Technol. A **32**, 031508 (2014); 10.1116/1.4870381

Single phase $In_xGa_{1-x}N$ ($0.25 \leq x \leq 0.63$) alloys synthesized by metal organic chemical vapor deposition


Appl. Phys. Lett. **93**, 182107 (2008); 10.1063/1.3006432

Morphological, electrical, and optical properties of InN grown by hydride vapor phase epitaxy on sapphire and template substrates



J. Appl. Phys. **99**, 116103 (2006); 10.1063/1.2201856

Influence of surface roughness and internal strain on defect spectrum and intensity of low-temperature photoluminescence of thin $Si_{1-x}Ge_x$ layers

J. Appl. Phys. **95**, 7681 (2004); 10.1063/1.1739288



Instruments for Advanced Science

<p>Contact Hiden Analytical for further details: W www.HidenAnalytical.com E info@hiden.co.uk CLICK TO VIEW our product catalogue</p>	 <p>Gas Analysis</p> <ul style="list-style-type: none"> › dynamic measurement of reaction gas streams › catalysis and thermal analysis › molecular beam studies › dissolved species probes › fermentation, environmental and ecological studies 	 <p>Surface Science</p> <ul style="list-style-type: none"> › UHV/TPD › SIMS › end point detection in ion beam etch › elemental imaging - surface mapping 	 <p>Plasma Diagnostics</p> <ul style="list-style-type: none"> › plasma source characterization › etch and deposition process reaction › kinetic studies › analysis of neutral and radical species 	 <p>Vacuum Analysis</p> <ul style="list-style-type: none"> › partial pressure measurement and control of process gases › reactive sputter process control › vacuum diagnostics › vacuum coating process monitoring
---	--	--	--	--

Low-temperature sequential pulsed chemical vapor deposition of ternary $B_xGa_{1-x}N$ and $B_xIn_{1-x}N$ thin film alloys

Ali Haider,^{a)} Seda Kizir, and Cagla Ozgit-Akgun

National Nanotechnology Research Center (UNAM), Bilkent University, Bilkent, Ankara 06800, Turkey
 and Institute of Materials Science and Nanotechnology, Bilkent University, Bilkent, Ankara 06800, Turkey

Ali Kemal Okyay

National Nanotechnology Research Center (UNAM), Bilkent University, Bilkent, Ankara 06800, Turkey;
 Institute of Materials Science and Nanotechnology, Bilkent University, Bilkent, Ankara 06800, Turkey;
 and Department of Electrical and Electronics Engineering, Bilkent University, Bilkent, Ankara 06800 Turkey

Necmi Biyikli^{a)}

National Nanotechnology Research Center (UNAM), Bilkent University, Bilkent, Ankara 06800, Turkey
 and Institute of Materials Science and Nanotechnology, Bilkent University, Bilkent, Ankara 06800, Turkey

(Received 5 September 2015; accepted 6 November 2015; published 18 November 2015)

In this work, the authors have performed sequential pulsed chemical vapor deposition of ternary $B_xGa_{1-x}N$ and $B_xIn_{1-x}N$ alloys at a growth temperature of 450 °C. Triethylboron, triethylgallium, trimethylindium, and N_2 or N_2/H_2 plasma have been utilized as boron, gallium, indium, and nitrogen precursors, respectively. The authors have studied the compositional dependence of structural, optical, and morphological properties of $B_xGa_{1-x}N$ and $B_xIn_{1-x}N$ ternary thin film alloys. Grazing incidence X-ray diffraction measurements showed that boron incorporation in wurtzite lattice of GaN and InN diminishes the crystallinity of $B_xGa_{1-x}N$ and $B_xIn_{1-x}N$ sample. Refractive index decreased from 2.24 to 1.65 as the B concentration of $B_xGa_{1-x}N$ increased from 35% to 88%. Similarly, refractive index of $B_xIn_{1-x}N$ changed from 1.98 to 1.74 for increase in B concentration value from 32% to 87%, respectively. Optical transmission band edge values of the $B_xGa_{1-x}N$ and $B_xIn_{1-x}N$ films shifted to lower wavelengths with increasing boron content, indicating the tunability of energy band gap with alloy composition. Atomic force microscopy measurements revealed an increase in surface roughness with boron concentration of $B_xGa_{1-x}N$, while an opposite trend was observed for $B_xIn_{1-x}N$ thin films. © 2015 American Vacuum Society.

[<http://dx.doi.org/10.1116/1.4936072>]

I. INTRODUCTION

Hexagonal boron nitride (hBN) thin films have attracted special attention due to their useful properties such as wide band gap, high thermal conductivity, high oxidation resistance, and low surface energy.^{1–3} On the other hand, GaN has been considered as one of the most important member of the III-nitride compound semiconductor material family, due to its superior electrical properties in addition to its robustness.⁴ Therefore, a hybrid of these superior properties might potentially be achieved via $B_xGa_{1-x}N$ ternary alloys. $B_xGa_{1-x}N$ can provide more degrees of freedom in fabricating optoelectronic device structures operating at shorter wavelengths.^{5,6} Hexagonal indium nitride ($hInN$), which has a direct band gap of ~ 0.7 eV, is also of significant interest because of its potential applications in optoelectronic devices, including high-electron mobility transistors, highly efficient multijunction solar cells, and infrared light-emitting diodes.^{7–12} $B_xIn_{1-x}N$, a ternary nitride semiconductor alloy that consists of hBN and $hInN$ can be employed in optoelectronic devices, which operates in a quite broad spectrum ranging from deep ultraviolet to infrared (200–1800 nm).¹³

However, these B-containing ternary III-nitride alloys have not been fully explored and exploited due to material

growth constraints and critical issues with phase control due to differences in crystalline structure and lattice parameters.¹⁴ hBN crystal features a layered structure of hexagonal sheets, whereas $hGaN$ and $hInN$ comprise a wurtzite hexagonal structure. If proper growth conditions are established to grow single phase $B_xGa_{1-x}N$ and $B_xIn_{1-x}N$ alloys, these materials might find a variety of applications in UV optoelectronics, high-temperature and radiation/power tolerant electronics.¹⁴ In addition, $B_xGa_{1-x}N$ can be used as a buffer layer for epitaxial lateral overgrowth of GaN to achieve low threading dislocation densities.⁶ It has been reported that when a certain boron concentration is exceeded, phase separation is being observed.¹⁴ There are few reports on growth of $B_xGa_{1-x}N$ and $B_xIn_{1-x}N$, which have been grown using high-temperature metal-organic vapor phase epitaxy and molecular beam epitaxy.^{13,14} Alloy thin films can be deposited either by regulating the vapor pressures of simultaneously exposed precursors or by designing a unit growth cycle that is made up of subcycles of the constituent materials and running in a cyclic process. The latter is termed as “digital alloying,” which is a straightforward method of accurately controlling the composition of thin film alloys. In our previous work, we had demonstrated the growth of $Al_xGa_{1-x}N$ (Ref. 15) and $In_xGa_{1-x}N$ (Ref. 16) thin films at growth temperature of 200 °C via plasma-assisted atomic layer deposition integrated with a hollow-cathode plasma

^{a)}Electronic addresses: ali.haider@bilkent.edu.tr; biyikli@unam.bilkent.edu.tr

source, where we changed the concentration of Al and In with digital alloying. In this work, we demonstrate the sequential pulsed chemical vapor deposition (CVD) of $B_xGa_{1-x}N$ and $B_xIn_{1-x}N$ thin films at substrate temperature of 450 °C. Triethylboron, triethylgallium, trimethylindium, and N_2 or N_2/H_2 plasma have been utilized as boron, gallium, indium, and nitrogen precursors, respectively. Structural, optical, and morphological characterization results are presented and discussed.

II. EXPERIMENT

A. Film growth

BN, GaN, InN, $B_xIn_{1-x}N$, and $B_xGa_{1-x}N$ thin films were deposited at 450 °C in a modified Fiji F200-LL remote-plasma ALD reactor (Ultratech/CambridgeNanoTech, Inc.) attached with an Adixen ACP 120G dry scroll vacuum pump, which was backed by an Adixen ATH 400 M turbo pump. The original RF power supply (Seren IPS, Inc., R301), matching network controller (Seren IPS, Inc., MC2), and automatic matching network (Seren IPS, Inc., AT-3) units were used to activate the hollow cathode plasma discharge. Solvent cleaning of silicon (Si) and double-side polished quartz substrates was performed by sequential ultrasonic agitation in 2-propanol, acetone, and methanol, followed by rinsing with de-ionized (DI) water and drying with N_2 . Si was submerged into dilute hydrofluoric acid solution for 2 min in order to remove the native oxide layer, followed by rinsing with DI water and drying with N_2 . Substrates were kept at deposition temperature for at least 20 min before the growth process was started. During the growth sessions, rotation speed of the Adixen ATH 400 M turbo pump was adjusted in order to keep the reactor pressure fixed at ~ 150 mTorr. Base pressure of the system was lower than 10^{-5} Torr.

Triethylboron (TEB), triethylgallium (TEG), and trimethylindium (TMI) were used as boron, gallium, and indium metal precursors. N_2/H_2 and N_2 plasma were used as nitrogen precursors for growth of GaN and InN films, respectively. Same nitrogen source was used for respective subcycles of GaN and InN in the main cycle of $B_xGa_{1-x}N$ and $B_xIn_{1-x}N$ thin film growth. BN growth with TEB and N_2/H_2 plasma as boron and nitrogen precursors, respectively, at 450 °C has been reported elsewhere.¹⁷ For $B_xGa_{1-x}N$ growth, N_2/H_2 plasma has been used as nitrogen source for subcycle of BN. However, as InN subcycle in $B_xIn_{1-x}N$ thin film uses N_2 plasma as nitrogen source, we have used N_2 plasma as nitrogen precursor for BN subcycle in $B_xIn_{1-x}N$ thin film growth in order to match the plasmas in the same growth run. Also, a separate growth run of BN was carried out using N_2 plasma as nitrogen source to compare the material properties of BN with $B_xIn_{1-x}N$ thin film alloys. Organometallic precursors and N_2/H_2 (or N_2) were carried from separate lines using 30 and 100 sccm Ar, respectively. TEG and TMI precursors were 99.999% pure, while TEB was $\geq 95\%$ pure. Initial purity of N_2-H_2 plasma gases and carrier gas, Ar was 99.999%, and these gases were further purified using MicroTorr gas purifiers. N_2/H_2 (or N_2) gas

flow rates and plasma power were kept constant in all experiments as 50/50 (50) sccm and 300 W, respectively. The system was purged for 10 s after each precursor exposure.

B. Film characterization

Grazing-incidence X-ray diffraction (GIXRD) patterns were recorded in an X'Pert PRO MRD diffractometer (PANalytical B.V., Almelo, Netherlands) using Cu K α radiation. Data were obtained within the 2Theta range of 20°–80° by the summation of ten scans, which were performed using 0.1° step size and 10 s counting time.

Elemental composition of the films were determined by X-ray photoelectron spectroscopy (XPS) using Thermo Scientific K-Alpha spectrometer (Thermo Fisher Scientific, Waltham, MA) with a monochromatized Al K α X-ray source. Atomic force microscope (AFM) (XE-100E, PSIA, Suwon, Korea) measurements were carried out in noncontact mode to reveal surface morphologies of the $B_xIn_{1-x}N$ and $B_xGa_{1-x}N$ thin films.

Spectral transmission measurements were carried out with a UV-VIS spectrophotometer (HR4000CG-UV-NIR, Ocean Optics, Inc., Dunedin, FL) in the wavelength range of 220–1000 nm relative to air. Optical constants of the films were determined using a variable angle spectroscopic ellipsometer (V-VASE, J.A. Woollam Co., Inc., Lincoln, NE), which is coupled with rotating analyzer and xenon light source. The ellipsometric spectra were collected at three angles of incidence (65°, 70°, and 75°) to yield adequate sensitivity over the full spectral range. Optical constants and film thicknesses were extracted by fitting the spectroscopic ellipsometry data. The numerical iteration was performed to minimize the mean-square error function using WVASE32 software (J.A. Woollam Co., Inc., Lincoln, NE). The homogeneous Tauc-Lorentz function was applied as an oscillator. Growth per cycle (GPC) values were computed by dividing film thicknesses to the number of growth cycles.

III. RESULTS AND DISCUSSION

$B_xGa_{1-x}N$ and $B_xIn_{1-x}N$ thin films with different boron compositions were deposited at 450 °C on precleaned Si (100) and double-side polished quartz substrates. In our previous work, we have reported growth of *h*BN thin film on silicon and quartz substrates with low impurities using TEB and N_2/H_2 plasma as boron and nitrogen precursors, respectively, in an hollow cathode plasma-assisted atomic layer deposition (HCPA-ALD) reactor.^{17,18} We were able to grow BN with appreciable GPC values at substrate temperatures of 350 and 450 °C. GPC values at 350 and 450 °C were 0.15 and 0.47 Å/cycle, respectively. BN thin films deposited in CVD regime at 350 and 450 °C were polycrystalline with hexagonal structure as determined by GIXRD and HR-TEM. Films exhibited an optical band edge at ~ 5.25 eV and high transparency ($>90\%$) in the visible region of the spectrum. A temperature of 450 °C was chosen for the growth of $B_xGa_{1-x}N$ and $B_xIn_{1-x}N$ alloys as growth per cycle of BN was substantially higher than the growth rates at lower

temperature ($<350^{\circ}\text{C}$). However, higher growth temperatures of BN ($>250^{\circ}\text{C}$) resulted in thermal decomposition of boron precursor (TEB). Thermal decomposition of precursor leads to CVD type growth at growth temperatures above a possible ALD growth temperature window. Keeping in mind the CVD growth of BN at 450°C , we have used the term sequential pulsed CVD in present case for growth of $\text{B}_x\text{Ga}_{1-x}\text{N}$ and $\text{B}_x\text{In}_{1-x}\text{N}$. Prior to growth of boron alloys, GaN and InN thin films were deposited at 450°C on Si (100) and double side polished quartz. GaN and InN thin films were used as reference samples to compare their material properties with $\text{B}_x\text{Ga}_{1-x}\text{N}$ and $\text{B}_x\text{In}_{1-x}\text{N}$ alloys. Recently, we have reported that InN growth at 200°C using N_2/H_2 plasma as nitrogen source results in a multiphase thin film composed of h -InN and t -InN phases with relatively high impurity (21 at. % oxygen) incorporation, whereas the film deposited using N_2 plasma reveals a single phase h -InN with substantially low impurity ($<2\%$ oxygen) content.¹⁹ In this work, we have carried out growth of InN at 450°C with N_2/H_2 plasma as nitrogen source, and no film growth was observed. Therefore, N_2 plasma was used as nitrogen source for the growth of InN film while N_2/H_2 plasma was used as nitrogen source for the growth of GaN film at 450°C . Metal and nitrogen precursors for growth of InN, BN, and GaN are summarized in Table I.

For $\text{B}_x\text{In}_{1-x}\text{N}$ growth, as explained in Sec. II, in order to keep the nitrogen source fixed as N_2 plasma, nitrogen plasma was used as N-precursor for BN subcycle. Additionally, a separate growth of BN thin film was carried out using TEB and N_2 plasma as boron and nitrogen precursors, respectively. Material properties of BN grown with N_2 plasma as nitrogen source were compared with $\text{B}_x\text{In}_{1-x}\text{N}$ thin film. The thickness values of GaN and InN thin films deposited at 450°C were measured using spectroscopic ellipsometer and were found to be ~ 35 (GPC = $0.70 \text{ \AA}/\text{cycle}$) and $\sim 38 \text{ nm}$ (GPC = $0.76 \text{ \AA}/\text{cycle}$), respectively. GPC of BN deposited using N_2/H_2 plasma at 450°C was $0.47 \text{ \AA}/\text{cycle}$.¹⁷ On the other hand, thickness of BN deposited at 450°C using N_2 plasma was 80 nm , which corresponds to GPC of $1.6 \text{ \AA}/\text{cycle}$. Having growth recipes of BN, InN, and GaN in hand, the total number of super-cycles was theoretically calculated for depositing $\sim 40 \text{ nm}$ of $\text{B}_x\text{Ga}_{1-x}\text{N}$ and $\text{B}_x\text{In}_{1-x}\text{N}$ with different compositions of boron. One super-cycle consisted of several subcycles of BN and GaN or InN, while the number of subcycles of binary films depends upon the desired concentration of alloy. The number of subcycles for a specific desired concentration of alloy was calculated using the following formula:

$$X_B = \frac{n_{\text{BN}} \text{GPC}_{\text{BN}}}{n_{\text{BN}} \text{GPC}_{\text{BN}} + n_{\text{GaN/InN}} \text{GPC}_{\text{GaN/InN}}}, \quad (1)$$

where X_B is concentration of boron, n_{BN} is number of BN subcycles, $n_{\text{GaN/InN}}$ is number of GaN or InN subcycles, and GPC is growth per cycle. Three different concentrations (Tables II and III) of boron were selected and the number of subcycles of BN and GaN or InN was calculated. The thickness values of $\text{B}_x\text{Ga}_{1-x}\text{N}$ thin films with 10%, 30%, and 50% boron extracted from spectroscopic ellipsometer measurements were 30, 37, and 43 nm, respectively. On the other hand, the thickness values of $\text{B}_x\text{In}_{1-x}\text{N}$ thin films extracted from spectroscopic ellipsometer measurements with 10%, 30%, and 50% boron were 29, 32, and 42 nm, respectively. The thickness values were close to the targeted value of 40 nm that was selected to compute the number of subcycles and super-cycles by Eq. (1). However, it is worth mentioning that the targeted calculation of alloy thickness and composition is not straightforward since the deposition rate of constituents of alloys (BN, GaN, or InN) might vary on different materials, i.e., GPC of BN on Si, BN, and GaN or InN might result in different values.

Table IV shows the composition of the B-III-N alloy contents, which were revealed by XPS measurements. $\text{B}_x\text{In}_{1-x}\text{N}$ alloys show boron concentration up to 87% while the minimum concentration of boron in $\text{B}_x\text{In}_{1-x}\text{N}$ alloys was 32%. $\text{B}_x\text{Ga}_{1-x}\text{N}$ alloys also show an increase in boron concentration from 35% to 88%. Based on XPS evaluation of alloy concentration values, $\text{B}_x\text{In}_{1-x}\text{N}$ alloys will be mentioned as $\text{B}_{0.32}\text{In}_{0.67}\text{N}$, $\text{B}_{0.75}\text{In}_{0.25}\text{N}$, and $\text{B}_{0.87}\text{In}_{0.13}\text{N}$. While $\text{B}_x\text{Ga}_{1-x}\text{N}$ alloys will be mentioned as $\text{B}_{0.35}\text{Ga}_{0.65}\text{N}$, $\text{B}_{0.76}\text{Ga}_{0.24}\text{N}$, and $\text{B}_{0.88}\text{Ga}_{0.12}\text{N}$. There is a variation between the targeted and evaluated composition by XPS. The resulting alloy composition might indicate two possible scenarios: (1) BN growth rate might be faster on GaN and InN layers when compared on Si or BN layer; (2) GaN and InN deposition on BN proceeds slower when compared to their growth on Si or GaN or InN layers.

The crystalline structure of $\text{B}_x\text{Ga}_{1-x}\text{N}$ and $\text{B}_x\text{In}_{1-x}\text{N}$ films was characterized by GIXRD (Fig. 1). Figure 1(a) shows the GIXRD patterns of $\text{B}_x\text{Ga}_{1-x}\text{N}$ thin films deposited on Si (100) substrates with different compositions. For comparison, GaN GIXRD pattern is also given. GaN thin film was polycrystalline with an hexagonal structure (ICDD reference code: 00-050-0792). There is one dominant reflection of hexagonal (002) crystallographic orientation, and two weakly pronounced reflections (101) and (100) appear as

TABLE I. Precursors used for growth of GaN, BN, InN, and ternary alloys.

Material	Metal precursor source	N_2 precursor source
BN (For $\text{B}_x\text{Ga}_{1-x}\text{N}$)	TEB	N_2/H_2 plasma
BN (For $\text{B}_x\text{In}_{1-x}\text{N}$)	TEB	N_2 plasma
GaN	TEG	N_2/H_2 plasma
InN	TMI	N_2 plasma

TABLE II. Calculation of number of subcycles of BN and GaN to deposit $\sim 40 \text{ nm}$ of $\text{B}_x\text{Ga}_{1-x}\text{N}$.

	$X_B = 0.1$	$X_B = 0.3$	$X_B = 0.5$
Number of BN subcycles	1	2	3
Number of GaN subcycles	6	3	2
Thickness of one super cycle (\AA)	4.67	3.04	2.81
Number of super cycles required to achieve a target thickness of $\sim 40 \text{ nm}$	86	132	143

TABLE III. Calculation of number of subcycles of BN and InN to deposit ~ 40 nm of $B_xIn_{1-x}N$.

	$X_B = 0.1$	$X_B = 0.3$	$X_B = 0.5$
Number of BN subcycles	1	1	1
Number of InN subcycles	18	4	2
Thickness of one super cycle (Å)	15.28	4.64	3.12
Number of super cycles required to achieve a target thickness of ~ 40 nm	26	86	128

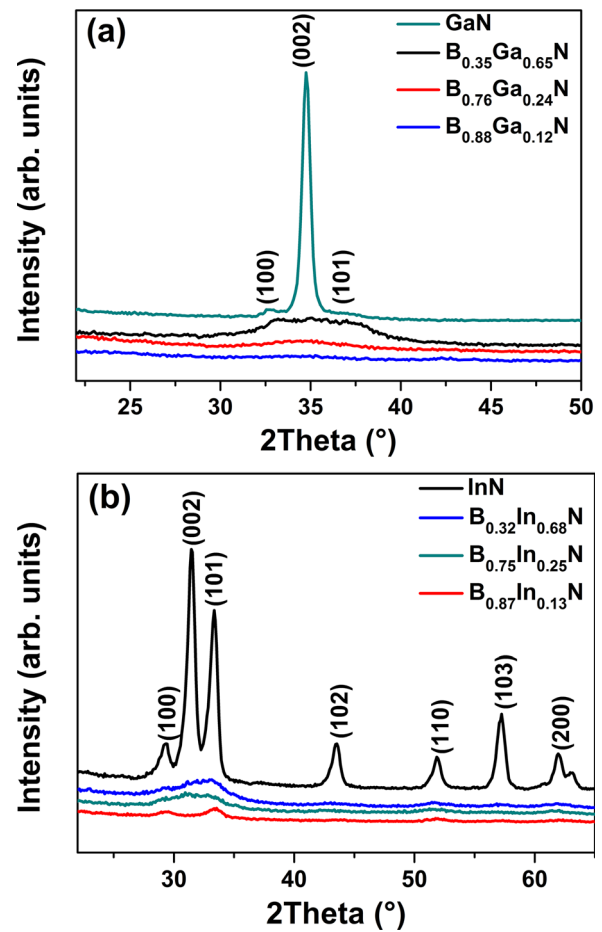
shoulders of the main peak. As soon as boron is incorporated in the films, the crystallinity of sample is diminished as revealed by a weak shoulder in the case of $B_{0.35}Ga_{0.65}N$ thin film, whereas $B_{0.76}Ga_{0.24}N$ and $B_{0.88}Ga_{0.12}N$ films showed amorphous character without any crystalline feature. Figure 1(b) shows the GIXRD patterns of $B_xIn_{1-x}N$ thin films deposited on Si (100) substrates with different compositions. The GIXRD pattern of InN was indexed to reflections from hexagonal wurtzite InN (ICDD reference code: 98-015-7515). Boron incorporation in wurtzite InN lattice destroyed the crystallinity of $B_xIn_{1-x}N$ films as GIXRD measurements of $B_{0.32}In_{0.68}N$, $B_{0.75}In_{0.25}N$, and $B_{0.87}In_{0.13}N$ reveal broad and less intense peaks. Keeping in view the structural dissimilarities of BN and GaN or InN, the results presented here depict that it is quite challenging to grow crystalline $B_xGa_{1-x}N$ and $B_xIn_{1-x}N$ alloys, especially at higher boron concentrations.

Figure 2(a) shows the spectral refractive index curves of BN, GaN, and $B_xGa_{1-x}N$ films deposited on Si(100). The refractive index value of BN grown at $450^\circ C$ using TEB and N_2/H_2 plasma was 1.61 at 550 nm; while for GaN grown at $450^\circ C$, it was measured to be 2.24 at 550 nm. The refractive index values of 1.6–1.7 has been reported in literature for BN thin films grown using plasma enhanced CVD,^{20,21} whereas 2.3–2.4 has been reported for GaN deposited using MOCVD.²² Refractive index decreased from 2.24 to 1.65 as the B concentration of $B_xGa_{1-x}N$ increased from 35% to 88%. The refractive index values of $B_{0.35}Ga_{0.65}N$, $B_{0.76}Ga_{0.24}N$, and $B_{0.87}Ga_{0.13}N$ samples were recorded as 2.06, 1.69, and 1.65, respectively.

Figure 2(b) shows a comparison of refractive index values of BN, InN, and $B_xIn_{1-x}N$ thin films deposited on Si(100). BN film deposited at $450^\circ C$ using TEB and N_2 plasma shows a refractive index value of 1.77 at 550 nm. On the other hand, the refractive index value was measured as 2.01 at 550 nm for InN film deposited at $450^\circ C$ using TMI and

TABLE IV. $B_xIn_{1-x}N$ and $B_xGa_{1-x}N$ alloy compositions calculated from XPS measurements.

Sample	B concentration	In concentration	Ga concentration
$B_xIn_{1-x}N$ (10%)	0.32	0.68	—
$B_xIn_{1-x}N$ (30%)	0.75	0.25	—
$B_xIn_{1-x}N$ (50%)	0.87	0.13	—
$B_xGa_{1-x}N$ (10%)	0.35	—	0.65
$B_xGa_{1-x}N$ (30%)	0.76	—	0.24
$B_xGa_{1-x}N$ (50%)	0.88	—	0.12

FIG. 1. (Color online) GIXRD pattern of (a) GaN and $B_xGa_{1-x}N$ with different compositions and (b) InN and $B_xIn_{1-x}N$ with different compositions.

N_2 plasma as indium and nitrogen precursors, respectively. Refractive index value of 2.5–2.6 has been reported in literature for InN thin films grown using magnetron sputtering.²³ As anticipated, the refractive index decreased from 1.98 to 1.74 as the boron concentration was increased from 32% to 87%. The results presented here shows that the refractive index values of $B_xGa_{1-x}N$ and $B_xIn_{1-x}N$ alloy thin films vary according to alloy composition.

Figure 3 shows optical transmission spectra of BN, GaN, InN, $B_xGa_{1-x}N$, and $B_xIn_{1-x}N$ thin films in UV-Vis and NIR regions deposited on double-side polished quartz substrates. The average transmittance for BN was measured to be 91%–93% range within the visible spectrum, which is close to bare quartz transmission value. This indicates that BN film is almost fully transparent in visible wavelength region. Decrease in transmission of BN thin film observed at UV wavelengths less than 280 nm was believed to be caused by the main band gap absorption.¹⁷ For GaN thin film [Fig. 3(a)], a significant decrease in the UV transmission was observed at wavelengths < 400 nm, which is most probably due to the main band-to-band absorption. InN thin film [Fig. 3(b)] exhibits 40%–50% transmission in the visible regime, which approaches up to 60%–70% in the NIR regime. The transmission values did not saturate for InN sample, possibly due to the relatively high impurity content and

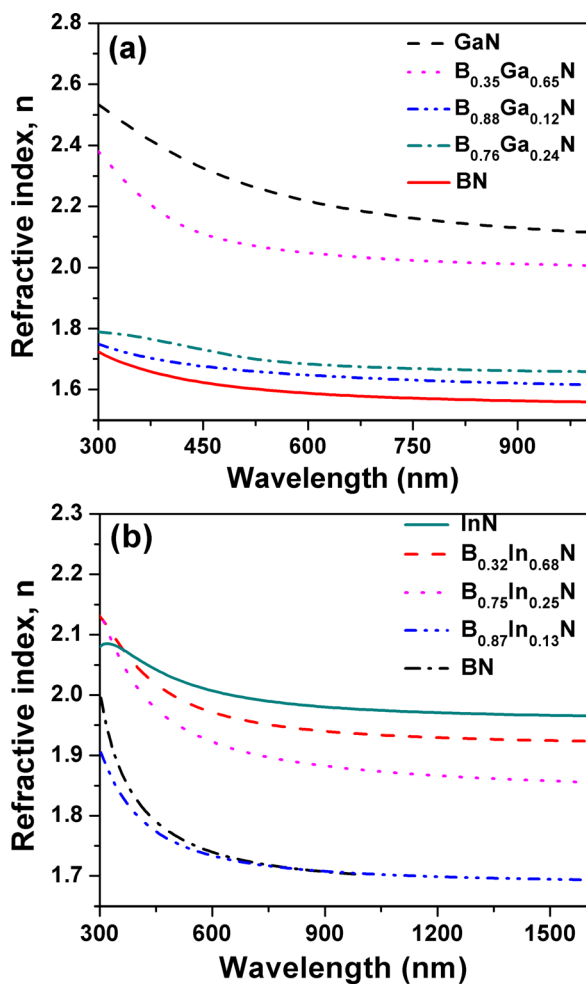


FIG. 2. (Color online) Refractive indices of (a) BN, GaN, and $B_xGa_{1-x}N$ with different compositions; (b) BN, InN and $B_xIn_{1-x}N$ with different compositions.

defect density present within the films.¹⁹ The transmission band edge values of the $B_xGa_{1-x}N$ and $B_xIn_{1-x}N$ thin films shifted to lower wavelengths with increasing boron content, demonstrating the successful tunability of optical band gap by changing alloy composition.

Surface morphologies of $B_xGa_{1-x}N$ and $B_xIn_{1-x}N$ samples were examined by AFM. Figures 4(a)–4(c) show the surface scans of the $B_{0.35}Ga_{0.65}N$, $B_{0.76}Ga_{0.24}N$, and $B_{0.88}Ga_{0.12}N$ thin films, respectively. Root-mean-square (Rms) roughness of $B_{0.35}Ga_{0.65}N$, $B_{0.76}Ga_{0.24}N$, and $B_{0.88}Ga_{0.12}N$ samples measured from $1 \times 1 \mu m$ scan area was 0.75, 3.52, and 4.68 nm, respectively. Previously, we have reported nonuniform, rough, compact, and three-dimensional (3D) curly surface morphology of BN.¹⁷ The rough morphology of BN might be the cause of increased roughness of $B_xGa_{1-x}N$ thin film alloys with an increase in boron concentration. Figures 4(d)–4(f) show the surface scans of the $B_{0.32}In_{0.68}N$, $B_{0.75}In_{0.25}N$, and $B_{0.87}In_{0.13}N$ thin films, respectively. Rms roughness of $B_{0.32}In_{0.68}N$, $B_{0.75}In_{0.25}N$, and $B_{0.87}In_{0.13}N$ samples was extracted as 5.84, 4.52, and 2.83 nm, respectively. These results imply a totally reverse trend in film surface roughness when compared with $B_xGa_{1-x}N$ samples. The main difference in the growth chemistry between $B_xIn_{1-x}N$

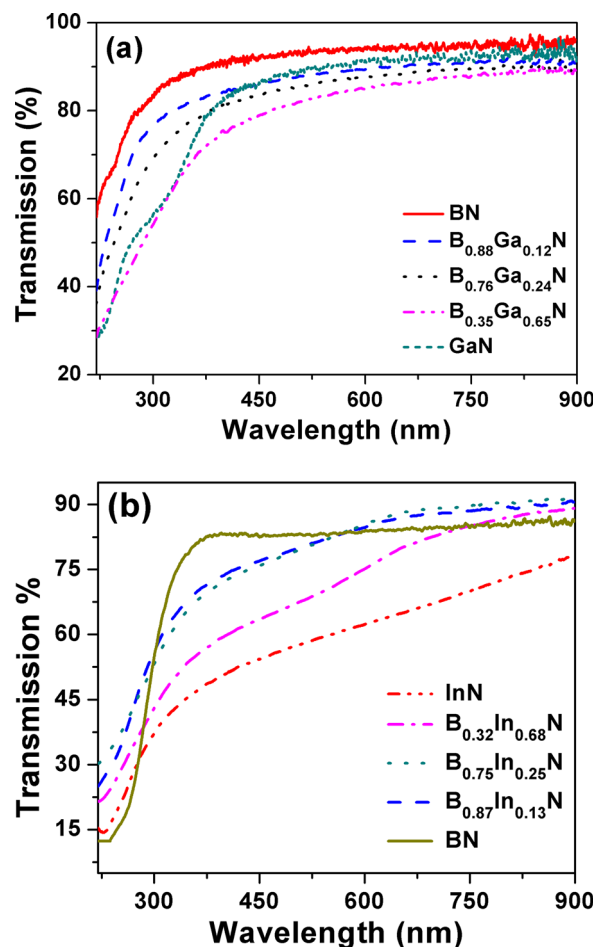


FIG. 3. (Color online) Transmission spectra of (a) BN, GaN, and $B_xGa_{1-x}N$ with different compositions; (b) BN, InN and $B_xIn_{1-x}N$ with different compositions.

and $B_xGa_{1-x}N$ lies in the choice of nitrogen precursor: N_2 plasma versus N_2/H_2 plasma. Therefore, it can be deduced that this plasma source difference shows a significant impact on the surface roughness of the resulting alloy films. Further systematic studies are needed to understand the possible mechanism behind the surface roughness of B(III)N alloys.

IV. SUMMARY AND CONCLUSIONS

$B_xGa_{1-x}N$ and $B_xIn_{1-x}N$ thin films have been grown on Si(100) and quartz substrates via sequential pulsed CVD technique in HCPA-ALD reactor at 450 °C. Individual GaN, InN, and BN subcycles have been tailored in the main ALD growth recipe to adjust the composition of $B_xGa_{1-x}N$ and $B_xIn_{1-x}N$ thin films. Grazing incidence X-ray diffraction measurements revealed that boron incorporation in wurtzite lattice of GaN and InN significantly diminishes the crystallinity in $B_xGa_{1-x}N$ and $B_xIn_{1-x}N$ samples. It is suspected that structural dissimilarities between BN and GaN or InN leads to amorphized $B_xGa_{1-x}N$ and $B_xIn_{1-x}N$ alloys at high boron concentrations. Spectroscopic ellipsometer measurements showed that refractive index varied from 2.24 to 1.65 as the B concentration of $B_xGa_{1-x}N$ increased from 32% to 87%. Similarly, the refractive index decreased from 1.98 to 1.74

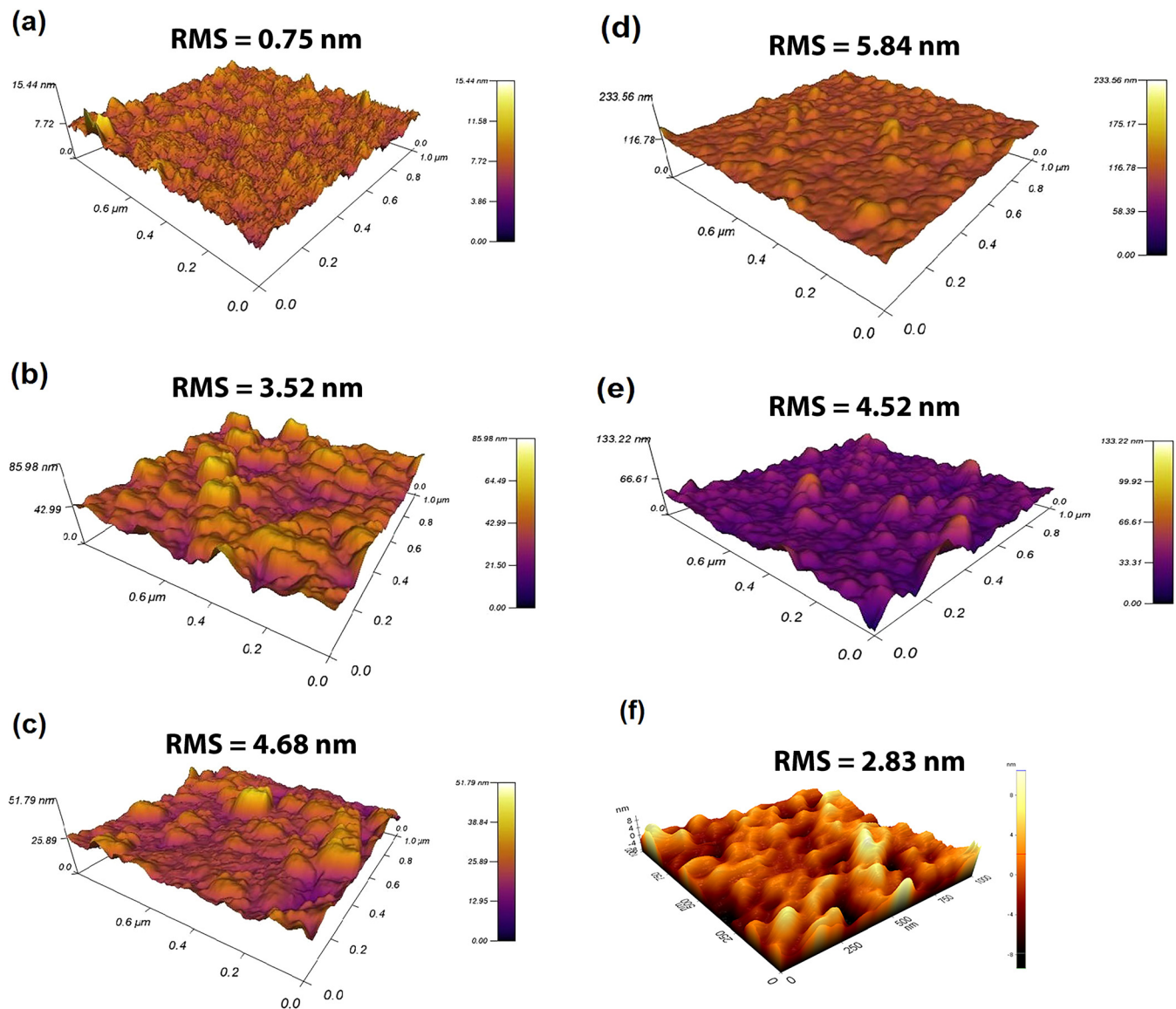


FIG. 4. (Color online) AFM images of (a) $B_{0.35}Ga_{0.65}N$, (b) $B_{0.76}Ga_{0.24}N$, (c) $B_{0.88}Ga_{0.12}N$, (d) $B_{0.32}In_{0.67}N$, (e) $B_{0.75}In_{0.25}N$, and (f) $B_{0.87}In_{0.13}N$.

as the B concentration of $B_xIn_{1-x}N$ increased from 35% to 88%. The shift of optical transmission band edge values of the $B_xGa_{1-x}N$ and $B_xIn_{1-x}N$ films to lower wavelengths with increasing boron contents confirmed the tunability of energy band gap with alloy composition. The atomic force microscopy measurements revealed an increase in surface roughness with boron content for $B_xGa_{1-x}N$, while an opposite trend was observed for $B_xIn_{1-x}N$ samples. This study demonstrates the monotonic variation of optical and structural properties of $B_xGa_{1-x}N$ and $B_xIn_{1-x}N$ with compositional digital alloying via sequential CVD technique employing a hollow-cathode plasma source.

ACKNOWLEDGMENTS

A. Haider acknowledges Higher Education Commission of Pakistan (HEC) for Human resource development (HRD) fellowship for M.S. leading to Ph.D. A. K. Okyay and N.

Biyikli acknowledge the financial support from TUBITAK (Project Nos. 112M482 and 214M015).

- ¹R. Paine and C. Narula, *Chem. Rev.* **90**, 73 (1990).
- ²K. Watanabe, T. Taniguchi, and H. Kanda, *Nat. Mater.* **3**, 404 (2004).
- ³K. Watanabe, T. Taniguchi, T. Niiyama, K. Miya, and M. Taniguchi, *Nat. Photonics* **3**, 591 (2009).
- ⁴S. C. Jain, M. Willander, J. Narayan, and R. Van Overstraeten, *J. Appl. Phys.* **87**, 965 (2000).
- ⁵C. H. Wei and J. H. Edgar, *J. Cryst. Growth* **217**, 109 (2000).
- ⁶T. Akasaka, Y. Kobayashi, and T. Makimoto, *J. Cryst. Growth* **298**, 320 (2007).
- ⁷S. F. Chichibu, T. Azuhata, M. Sugiyama, T. Kitamura, Y. Ishida, H. Okumura, H. Nakanishi, T. Sota, and T. Mukai, *J. Vac. Sci. Technol. B Microelectron.* **19**, 2177 (2001).
- ⁸J. J. Wierer *et al.*, *Appl. Phys. Lett.* **78**, 3379 (2001).
- ⁹B.-H. Chu *et al.*, *J. Vac. Sci. Technol. B* **28**, L5 (2010).
- ¹⁰Y. Bu, L. Ma, and M. C. Lin, *J. Vac. Sci. Technol. A* **11**, 2931 (1993).
- ¹¹T. Matsuoka, H. Okamoto, M. Nakao, H. Harima, and E. Kurimoto, *Appl. Phys. Lett.* **81**, 1246 (2002).
- ¹²R. Ascázubi, I. Wilke, K. Denniston, H. Lu, and W. J. Schaff, *Appl. Phys. Lett.* **84**, 4810 (2004).

- ¹³L. C. Chen and C. H. Tien, *Jpn. J. Appl. Phys.* **48**, 101001 (2009).
- ¹⁴G. Orsal, N. Maloufi, S. Gautier, M. Alnot, A. A. Sirenko, M. Bouchaour, and A. Ougazzaden, *J. Cryst. Growth* **310**, 5058 (2008).
- ¹⁵C. Ozgit-Akgun, E. Goldenberg, A. K. Okyay, and N. Biyikli, *J. Mater. Chem. C* **2**, 2123 (2014).
- ¹⁶A. Haider, S. Kizir, C. Ozgit, E. Goldenberg, S. A. Leghari, A. K. Okyay, and N. Biyikli, *J. Mater. Chem. C* **3**, 9620 (2015).
- ¹⁷A. Haider, C. Ozgit-Akgun, E. Goldenberg, A. K. Okyay, and N. Biyikli, *J. Am. Ceram. Soc.* **97**, 4052 (2014).
- ¹⁸A. Haider, C. Ozgit-Akgun, F. Kayaci, A. K. Okyay, T. Uyar, and N. Biyikli, *APL Mater.* **2**, 096109 (2014).
- ¹⁹C. Ozgit-Akgun, E. Goldenberg, S. Bolat, B. Tekcan, F. Kayaci, T. Uyar, A. K. Okyay, and N. Biyikli, *Phys. Status Solidi* **12**, 394 (2015).
- ²⁰T. A. Anutgan, M. Anutgan, I. Atilgan, and B. Katircioglu, *Thin Solid Films* **518**, 419 (2009).
- ²¹A. Abdellaoui, A. Bath, B. Bouchikhi, and O. Baehr, *Mater. Sci. Eng. B* **47**, 257 (1997).
- ²²G. Yu, G. Wang, H. Ishikawa, M. Umeno, T. Soga, T. Egawa, J. Watanabe, and T. Jimbo, *Appl. Phys. Lett.* **70**, 3209 (1997).
- ²³L. F. Jiang, W. Z. Shen, H. F. Yang, H. Ogawa, and Q. X. Guo, *Appl. Phys. A Mater. Sci. Process.* **78**, 89 (2004).